

**MASTER COPY:** PLEASE KEEP THIS "MEMORANDUM OF TRANSMITTAL" BLANK FOR REPRODUCTION PURPOSES. WHEN REPORTS ARE GENERATED UNDER THE ARO SPONSORSHIP, FORWARD A COMPLETED COPY OF THIS FORM WITH EACH REPORT SHIPMENT TO THE ARO. THIS WILL ASSURE PROPER IDENTIFICATION. NOT TO BE USED FOR INTERIM PROGRESS REPORTS; SEE PAGE 2 FOR INTERIM PROGRESS REPORT INSTRUCTIONS.

**MEMORANDUM OF TRANSMITTAL**

U.S. Army Research Office  
ATTN: AMSRL-RO-BI (TR)  
P.O. Box 12211  
Research Triangle Park, NC 27709-2211

Reprint (Orig + 2 copies)

Technical Report (Orig + 2 copies)

Manuscript (1 copy)

Final Progress Report (Orig + 2 copies)

Related Materials, Abstracts, Theses (1 copy)

CONTRACT/GRANT NUMBER:

REPORT TITLE:

is forwarded for your information.

SUBMITTED FOR PUBLICATION TO (applicable only if report is manuscript):

Sincerely,

# REPORT DOCUMENTATION PAGE

Form Approved  
OMB NO. 0704-0188

Public Reporting burden for this collection of information is estimated to average 1 hour per response, including the time for reviewing instructions, searching existing data sources, gathering and maintaining the data needed, and completing and reviewing the collection of information. Send comment regarding this burden estimates or any other aspect of this collection of information, including suggestions for reducing this burden, to Washington Headquarters Services, Directorate for information Operations and Reports, 1215 Jefferson Davis Highway, Suite 1204, Arlington, VA 22202-4302, and to the Office of Management and Budget, Paperwork Reduction Project (0704-0188,) Washington, DC 20503.

1. AGENCY USE ONLY ( Leave Blank)		2. REPORT DATE		3. REPORT TYPE AND DATES COVERED	
4. TITLE AND SUBTITLE				5. FUNDING NUMBERS	
6. AUTHOR(S)					
7. PERFORMING ORGANIZATION NAME(S) AND ADDRESS(ES)				8. PERFORMING ORGANIZATION REPORT NUMBER	
9. SPONSORING / MONITORING AGENCY NAME(S) AND ADDRESS(ES)  U. S. Army Research Office P.O. Box 12211 Research Triangle Park, NC 27709-2211				10. SPONSORING / MONITORING AGENCY REPORT NUMBER	
11. SUPPLEMENTARY NOTES The views, opinions and/or findings contained in this report are those of the author(s) and should not be construed as an official Department of the Army position, policy or decision, unless so designated by other documentation.					
12 a. DISTRIBUTION / AVAILABILITY STATEMENT  Approved for public release; distribution unlimited.				12 b. DISTRIBUTION CODE	
13. ABSTRACT (Maximum 200 words)					
14. SUBJECT TERMS				15. NUMBER OF PAGES	
				16. PRICE CODE	
17. SECURITY CLASSIFICATION OR REPORT <b>UNCLASSIFIED</b>		18. SECURITY CLASSIFICATION ON THIS PAGE <b>UNCLASSIFIED</b>		19. SECURITY CLASSIFICATION OF ABSTRACT <b>UNCLASSIFIED</b>	
				20. LIMITATION OF ABSTRACT <b>UL</b>	

NSN 7540-01-280-5500

Standard Form 298 (Rev.2-89)  
Prescribed by ANSI Std. 239-18  
298-102

Enclosure 1

# Information Efficiency and Transmission Range Optimization for Coded MIMO FH-CDMA Ad Hoc Networks in Time-Varying Environment

Haichang Sui and James R. Zeidler

Dept. of Electrical & Computer Engineering,

Univ. of California, San Diego, La Jolla, CA 92093-0407

Emails: haichangsui@gmail.com, zeidler@ece.ucsd.edu

## ABSTRACT

Optimization of the transmission range in terms of maximizing information efficiency is studied in this paper for mobile ad hoc networks with frequency-hopped (FH) CDMA and multiple antennas. Realistic channel models are employed to account for path-loss, log-normal shadowing, and Rayleigh fading. The shadowing and fading are assumed time-varying due to mobility and hopping. The receiver performs decision-feedback demodulation for differential unitary space-time modulation and erasure insertion decoding for Reed-Solomon codes [13] [14]. The decoding error probability is derived based on distributions of the multiple access interference power and the SIR in a dwell for ground propagation model (path-loss exponent equal to 4). The trade-off between information efficiency and transmission range is studied in details and insights are obtained on the impact of various factors, including the spreading gain, modulation and coding schemes, feedback length, erasure insertion, order of spatial diversity, time-variation of the shadowing, and channel statistics such as Doppler frequency and shadowing spread.

This work is supported by, or in part by, the U. S. Army Research Office under the Multi-University Research Initiative (MURI) grant # W911NF-04-1-0224, the Office of Naval Research (Code 313), and the UCSD Center for Wireless Communications (UC IUCRP grant #03-10148)

*Index Terms* MIMO, frequency-hopped (FH) CDMA, erasure insertion, mobile ad hoc network (MANET), information efficiency, optimum transmission range, Gaussian quadrature

## I. INTRODUCTION

Frequency-hopped (FH) CDMA has been utilized for packet radio networks [1] [2] and adopted in IEEE 802.11 and 802.15 standards. It is also considered for the future IEEE 802.20 standards. Among its advantages are anti-jamming, low probability of interception/detection, and operability in non-continuous spectrum. In addition, FH is robust to the near-far problem, while its direct-sequence (DS) counterpart requires either accurate power-control [3] [4] or multi-user detection [5] [6] [7]. For several fading models, performance comparison between FH and DS systems also favors the former in distributed multiple-access networks [8] [9] [10] [11] [12].

A Reed-Solomon (RS) coded FH-CDMA transceiver structure with MIMO is developed in [13] [14] for mobile ad hoc network (MANET) applications, where differential unitary space-time modulation (DUSTM) is used to achieve spatial diversity in time-varying channel without channel state information at the receiver (CSIR) [39]. Decision-feedback demodulation (DFD), decision-directed adaptive estimation, and erasure insertion (EI) decoding operate interactively to improve demodulation, estimate symbol reliability, and suppress interference. The proposed system has the advantages of being robust to high mobility and unknown interference, in contrast to other work on applying MIMO to MANET [15] [16] [17] [18] [19] [20] which may be sensitive to inaccurate CSIR or synchronization errors [21].

Superior near-far resistance observed in the link performance reported by [13] [14] motivates us to further investigate network performance with the proposed physical layer (PHY). In particular, we are interested in determining the optimum transmission range (or equivalently the transmission power), which is related to network connectivity and hop length. For example, larger transmission range translates to fewer hops for a packet to reach its destination but also more interference to neighboring nodes, while short transmission range limits interference and allows spatial reuse [26] but incurs overhead in relaying/routing. Such a trade-off between forward progress and interference certainly depends on the interference suppression capability of the node and the channel model. Assuming that a packet can be successfully received as long as it is sent within a critical radius and no other active transmissions in that range (i.e., the so-called “collision model” without capture or path-loss/shadowing/fading), geometrical analysis showed that the

number of nodes in the optimum critical radius is between six and eight [22] [23] [24] [25] [26]. For DS-CDMA networks with single-user receiver and a path-loss channel model, Sousa and Silvester [27] derived that the optimal number of nodes that are closer to the receiver than the transmitter is related to the spreading gain due to power capture and CDMA. The results in [27] are further extended by Zorzi and Pupolin to include shadowing and fading in the channel model [28] [29]. On the other hand, a larger transmission range may lead to lower spectral efficiency since more redundancy is required for reliable communication over a long distance. Therefore, more insight into network design may be revealed by considering the so-called *information efficiency* (IE) [33], expressed as the forward progress multiplied by the throughput. Similarly, the trade-off between IE and transmission range also depends on the signal waveform, the receiver structure, and the channel model. Optimizing the transmission range to maximize IE is studied for DS-CDMA networks in [30].

A distinct feature of FH systems is that, due to hopping and interleaving, the coded symbols corresponding to the same codeword are subject to different signal-to-interference-ratio (SIR) levels. Such “interference diversity” can be exploited by proper coding and interleaving to effectively suppress multiple-access interference (MAI) in FH-CDMA networks [13] [14] [36]. In contrast, symbols in the same packet are usually subject to the same SIR level in narrow-band or DS-CDMA networks and the packet successful probability in these scenarios are commonly determined by a threshold test on the SIR in a packet [12] [27] [28] [29] [30] [31] [32].

In this paper, the trade-off between IE and transmission range is studied for FH-CDMA network with the transceiver structure proposed in [13] [14] under realistic time-varying channel model accounting for path-loss, log-normal shadowing, and Rayleigh fading. Previous studies of similar problems include [34] [35], which consider FSK and RS coding without EI decoding and/or shadowing. Another related work is [36], where bit-interleaved coded modulation and coherent demodulation are assumed. The impact of mobility on network design and the effect of shadowing time-scale revealed here are not available in [28] [29] [30] [31] [32] [33] [34] [35] [36]. Optimum modulation and coding schemes (MCSs) are also found for different system settings, which offers guidance for adaptive transmissions. Our results shed light on how the network performance depends on various design parameters and channel properties, including MCS, the number of antennas, receiver algorithms, spreading gain, dwell length, Doppler frequency, and shadowing spread/speed.

The rest of the paper is organized as following. The system model is presented in Section II. In Section III, packet error probability and IE are derived. The trade-off between IE and the transmission range, together with the effects of various system parameters, are studied in detail in Section IV and Section V concludes the paper.

## II. SYSTEM MODEL

### A. Network Model

We assume a network with nodes randomly distributed over the plane according to a two-dimensional Poisson point process with parameter  $\lambda$ . That is, the probability of having  $k$  nodes in a region with area  $A$  is given by  $\frac{1}{k!} (\lambda A)^k e^{-\lambda A}$ . Without loss of generality, we consider the link between two generic nodes  $\mathcal{S}$  and  $\mathcal{D}$  in Fig. 1, which are separated by distance  $R$ . To focus on an interference-limited network without power-control, we ignore AWGN and set the transmit power of all nodes to be unity. Nodes access the channel according to the slotted-ALOHA protocol and the transmission probability is denoted by  $p$ . For FH-CDMA networks, carrier frequency of a user changes periodically according to some pseudo-random hopping pattern. The total number of carrier frequencies that a hopped signal can be transmitted on, i.e. the spreading gain, is denoted by  $q$  and the carrier spacing is denoted by  $\Delta f$ .

### B. Transceiver and Channel Model (PHY)

The PHY transceiver structure for node  $\mathcal{S}$  and  $\mathcal{D}$  is specified in details in [13] [14]. The transmitter model is depicted as in Fig.2. Information bits are coded by  $(L, K)$  RS code and the coded symbols are then modulated by DUSTM. For simplicity, we assume the codeword length  $L$  is also the size of the DUSTM constellation  $\mathcal{V} = \{\mathbf{V}_0, \dots, \mathbf{V}_{L-1}\}$ , where  $\{\mathbf{V}_l\}_{l=0}^{L-1}$  are  $N_T \times N_T$  unitary matrices and  $N_T$  is the number of transmit antennas of node  $\mathcal{S}$  [39]. Design criteria and examples of  $\{\mathbf{V}_l\}_{l=0}^{L-1}$  have been extensively studied, e.g. [40] and references therein. By denoting the  $\tau$ th coded symbol as  $z_\tau$  ( $z_\tau = 0, \dots, L-1$ ), the corresponding space-time signal to be transmitted is an  $N_T \times N_T$  unitary matrices generated by differential modulation  $\mathbf{S}_{0,\tau} = \mathbf{V}_{z_\tau} \mathbf{S}_{0,\tau-1}$ . The length of a DUSTM block is denoted by  $T_s$  and  $\mathbf{S}_{0,\tau}$  is transmitted in the  $\tau$ th block by one of the  $q$  carrier frequencies. The hopping rate is assumed to be  $\frac{1}{N_c T_s}$  for some positive integer  $N_c > 1$  (slow FH) and the interval between hops is referred as a dwell. The interleaver and packet format are the same as in [13] [14] [34]. Specifically, a packet contains

multiple frames while each frame consists of  $N_c$  RS codewords, which are interleaved such that the  $L$  coded symbols from the same codeword are transmitted in different dwells to achieve frequency diversity.

The wireless channel between two arbitrary nodes is subject to deterministic path-loss and time-varying shadowing and fading. Formally, the channel gain can be written as  $d^{-b/2} \cdot \sqrt{S(t)} \cdot h(t)$  where  $d$  is the distance between the two nodes,  $b$  is the path-loss exponent normally in the range of 2 to 4 [44],  $S(t)$  is a log-normal random variable (r.v.) representing shadowing, and  $h(t)$  is circular symmetric complex (c.s.c.) Gaussian due to Rayleigh fading. Assuming that  $\mathcal{D}$  successfully locks onto the hopping pattern of  $\mathcal{S}$  according to certain spread spectrum protocols (e.g. [37] [38]), the received space-time signal  $\mathbf{R}_\tau$  in the  $\tau$ th DUSTM block after dehopping can be written as an  $N_T \times N_R$  matrix with each column containing data samples received on one of the  $N_R$  antennas. That is

$$\mathbf{R}_\tau = R^{-b/2} \sqrt{S_0(\tau)} \mathbf{S}_{0,\tau} \mathbf{H}_{0,\tau} + \mathbf{R}_{MAI,\tau} . \quad (1)$$

In (1), the two terms on the right hand side correspond to the desired signal and MAI, respectively. The transmission range  $R$  is the distance between  $\mathcal{S}$  and  $\mathcal{D}$ , while  $S_0(\tau)$  represents the log-normal shadowing for the  $\mathcal{S}$ - $\mathcal{D}$  link with the probability density function (pdf)

$$f_S(s) = \frac{1}{\sqrt{2\pi}\sigma_s s} \exp\left(-\frac{(\ln y)^2}{2\sigma_s^2}\right), \quad (2)$$

where  $\frac{10}{\ln 10} \sigma_s$  is the shadowing spread expressed in decibel [44]. The  $N_T \times N_R$  channel matrix  $\mathbf{H}_{0,\tau}$  contains the Rayleigh fading coefficients between all  $N_T N_R$  antenna pairs, which are i.i.d. c.s.c. Gaussian r.v.s with zero mean and unit variance (no spatial correlation).

The receiver proposed in [13] [14] performs DFD, decision-directed adaptive estimation, and EI decoding interactively, as shown in Fig.3. The DFD for DUSTM collects the received signal  $\mathbf{R}_\tau, \dots, \mathbf{R}_{\tau-P}$  in  $P+1$  blocks, together with the feedback decisions  $\hat{z}_{\tau-1}, \dots, \hat{z}_{\tau-P+1}$ , to demodulate the transmitted symbol  $z_\tau$  as the following ([13] [14]):

$$\hat{z}_\tau = \arg \max_{k=0, \dots, L-1} \lambda_{\tau,k}, \quad (3)$$

where

$$\lambda_{\tau,k} = -\frac{1}{\hat{\sigma}_{P,\tau}^2} \left\| \mathbf{V}_k^H \mathbf{R}_\tau - \sum_{j=1}^P \hat{a}_{j,\tau} \left( \prod_{t=\tau-j+1}^{\tau-1} \mathbf{V}_{\hat{z}_t} \right) \mathbf{R}_{\tau-j} \right\|^2 \quad (4)$$

The coefficients  $\hat{a}_{1,\tau}, \dots, \hat{a}_{P,\tau}$  and  $\hat{\sigma}_{P,\tau}^2$  in (4) are adaptively updated by the decision-directed RLS algorithm in Fig.3. Details on the algorithm can be found in [13] [14] and will not be presented here. In this paper, EI based on the so-called *effective SIR* (ESIR) [13] is considered. The ESIR is formulated in Section III-A by examining the pairwise error probability of the DFD [42]. In practice, it is estimated by

$$\hat{\rho}_{\text{eff},\tau} \triangleq \frac{\hat{P}_{\text{tot},\tau}}{\hat{\sigma}_{P,\tau}^2} - 1 \quad (5)$$

where

$$\hat{P}_{\text{tot},\tau} = \hat{P}_{\text{tot},\tau-1} + \frac{1-\mu}{N_T N_R} \|\mathbf{R}_\tau\|_F^2 \quad (6)$$

is the estimate of total received signal plus interference power [13]. In (6), the notation  $\|\cdot\|_F$  denotes the Frobenius norm of a matrix and  $\mu$  is the forgetting factor. The demodulated symbol  $\hat{z}_\tau$  in (3) is replaced by an erasure if the threshold test

$$\hat{\rho}_{\text{eff},\tau} \leq \rho_{\text{eth}} \quad (7)$$

is satisfied. Since the reliability of DFD can be measured by the ESIR [42], the decoding error probability may be significantly improved by choosing  $\rho_{\text{eth}}$  appropriately [13]. The IE with and without the ESIR threshold test (ESTT) EI will be analyzed in Section III.

An important consideration in performance analysis is the time-variation of the channel due to mobility and hopping. The time-scales of variation are significantly different for different channel effects. In this paper, the relative distance between nodes, i.e. the network topology, is assumed invariant in a packet duration as in [22] [23] [24] [25] [26] [27] [28] [29] [30] [31] [32] [33] [34] [35] [36]. The Rayleigh fading is modelled to be time-varying across DUSTM blocks and constant within each block for analytic tractability. Although analysis in the sequel applies for arbitrary time-correlation of the Rayleigh fading, we employ the Jakes' model [45] so that the correlation sequence is solely parameterized by the normalized Doppler frequency  $f_d T_s$ . Furthermore, we consider two scenarios for the time-scale of shadowing variation relative to the

dwell length. For *fast shadowing*, the coherence time of  $S_0(\tau)$  is taken to be the dwell length and the  $\mathcal{S}$ - $\mathcal{D}$  link experiences independent shadowing for different dwells. For *slow shadowing*, the random process  $S_0(\tau)$  is assumed to be constant for the whole packet as in [33] [34] [35] [36]. Thus, the coherence time of  $S_0(\tau)$  is at least  $L \cdot N_c T_s$ . It is clear that whether a specific shadowing process is fast or slow time-varying depends not only on the mobility but also on the length of the dwell.

### C. Interference Model

Heavy traffic model, i.e. nodes always having packets to transmit, is employed as in [22] [23] [24] [25] [26] [27] [28] [29] [30] [31] [32] [33] [34] [35] [36]. Thus, interfering nodes are randomly distributed over the plane according to a two-dimensional Poisson point process with parameter  $\lambda' = \lambda p/q$ . For clarity, we assume dwell synchronization so that the MAI process  $\{\mathbf{R}_{MAI,\tau}\}_\tau$  is stationary in a dwell, although the receiver proposed in [13] [14] can adaptively track non-stationarity due to dwell-asynchronism. The MAI  $\mathbf{R}_{MAI,\tau}$  can be formally defined as

$$\mathbf{R}_{MAI,\tau} = \lim_{a \rightarrow \infty} \mathbf{R}_{MAI,\tau}(a) \quad (8)$$

where  $\mathbf{R}_{MAI,\tau}(a)$  denotes the MAI resulted from nodes in a circle centered at node  $\mathcal{D}$  with radius  $a$ , which is given by

$$\mathbf{R}_{MAI,\tau}(a) = \sum_k^{\lceil \lambda' \pi a^2 \rceil} d_k^{-b/2} \sqrt{S_k(\tau)} \mathbf{S}_{k,\tau} \mathbf{H}_{k,\tau} . \quad (9)$$

In (9), the notation  $\sum^{\lceil N'_0 \rceil}$  refers to a sum whose number of summands is a Poisson r.v. with mean  $N'_0$ . The r.v.  $d_k$  and  $S_k(\tau)$  in (9) are the distance and log-normal shadowing (with pdf (2)) of the interferer- $\mathcal{D}$  link respectively. The interference signal matrix  $\mathbf{S}_{k,\tau}$  is  $N_T \times N_{T,k}$  and the Rayleigh fading matrix  $\mathbf{H}_{k,\tau}$  is  $N_{T,k} \times N_R$ , where  $N_{T,k}$  denotes the number of transmit antennas of the corresponding interfering node.

For a given dwell, Gaussian approximation is employed for elements in  $\mathbf{S}_{k,\tau} \mathbf{H}_{k,\tau}$ , whose variance is normalized to unity to account for equal transmit power of nodes in the network. The interference signal after Rayleigh fading  $\mathbf{S}_{k,\tau} \mathbf{H}_{k,\tau}$  is further assumed to be independent for different  $k$ s and uncorrelated in space and time. Thus, by conditioning on the distance and

shadowing for all interferer- $\mathcal{D}$  links, elements in  $\mathbf{R}_{MAI,\tau}(a)$  are i.i.d. c.s.c. Gaussian r.v.s with zero mean and squared variance given by

$$\sigma_w^2(a) \triangleq \sum_k^{[\lambda\pi a^2]} d_k^{-b} S_k. \quad (10)$$

In (10), time dependence of the shadowing is not explicitly shown because it is constant within a dwell in both the fast and slow shadowing model. Furthermore, under random hopping and dwell synchronization, the probability of two different dwells are hit by the same interfering nodes becomes negligible for large  $q$  and we may assume the set of interfering nodes to be independent for different dwells. Consequently, we will model the MAI  $\mathbf{R}_{MAI,\tau}$  in a dwell as a stationary c.s.c. Gaussian process uncorrelated in space and time when conditioned on its variance

$$\sigma_w^2 \triangleq \lim_{a \rightarrow \infty} \sigma_w^2(a), \quad (11)$$

which is itself an i.i.d. r.v. for each dwell.

### III. INFORMATION EFFICIENCY AND OPTIMUM TRANSMISSION RANGE

In this section, we use the IE [33] [34] as the objective function to optimize the transmission range  $R$ , or equivalently the expected number of nodes closer to  $\mathcal{D}$  than  $\mathcal{S}$ , i.e.,  $N_0 \triangleq \lambda\pi R^2$ . As in [33] [34], the IE is defined by

$$IE \triangleq \tau(p) \cdot (1 - P_E) \cdot \xi \cdot R, \quad (12)$$

where  $\tau(p)$  is the probability that  $\mathcal{S}$  and  $\mathcal{D}$  choose each other to communicate, or the "tendency to pair-up", which is derived in [27] to be

$$\tau(p) = (1 - p) (1 - e^{-p}). \quad (13)$$

In (12),  $\xi$  is the spectral efficiency (bits/sec/Hz) which, after trivial scaling, is given by

$$\xi = \frac{1}{q} \frac{K}{L} \log_2(L). \quad (14)$$

The packet error probability is denoted by  $P_E$  in (12). Furthermore, we use the decoding error probability  $P_C$  to approximate  $P_E$ , which is reasonable when the multiple codeword error events in the same packet are highly correlated.

In the rest of this section, we will first briefly review the results on ESIR and symbol error probability derived in [42] by conditioning on the received SIR in a given dwell. The received SIR  $\rho$  can be written as

$$\rho = \frac{R^{-b} S_0}{\sigma_w^2} \quad (15)$$

where  $S_0$  and  $\sigma_w^2$  are the log-normal shadowing and MAI power in a given dwell. Then we derive the pdf of MAI power  $\sigma_w^2$ . Finally, the distribution of  $\rho$  is derived and the decoding error probability  $P_C$  is obtained based on the resulting distribution and the conditional symbol error/erasure probabilities.

#### A. Symbol error/erasure probability

The performance of DUSTM with DFD is analyzed in [42]. When feedback errors are ignored, the pairwise error probability is given by

$$\begin{aligned} P_{k,l}(\rho) &\triangleq \Pr \{ \widehat{z}_\tau = k | z_\tau = l \} \\ &= \frac{1}{\pi} \int_0^{\pi/2} \prod_{m=1}^{N_T} \left[ 1 + \frac{\rho_{\text{eff}}(\rho) \sigma_{m,k,l}^2}{4 \cos^2 \theta} \right]^{-N_R} d\theta. \end{aligned} \quad (16)$$

where  $\sigma_{m,k,l}$  ( $m = 1, \dots, N_T$ ) is the  $m$ th singular value of the matrix  $\mathbf{V}_k - \mathbf{V}_l$ . The pre-EI symbol error probability can be approximated by the union bound as

$$P_e(\rho) \cong \frac{1}{L} \sum_{l=0}^{L-1} \sum_{k=0, k \neq l}^{L-1} P_{k,l}(\rho) \quad (17)$$

The ESIR  $\rho_{\text{eff}}(\rho)$  in (16) accounts for the time-correlation of Rayleigh fading and the feedback length  $P$ . As is shown in [42], it can be expressed compactly as

$$\rho_{\text{eff}}(\rho) = \frac{P_R + \sigma_w^2}{\sigma_P^2} - 1. \quad (18)$$

where  $P_R \triangleq R^{-b} S_0$  is the received signal power. The term  $\sigma_P$  in (18) is the  $P$ -th order minimum linear prediction error variance of the Gaussian random process  $\left\{ [\mathbf{H}_{0,\tau}]_{m,n} + [\mathbf{R}_{MAI,\tau}]_{m,n} \right\}_\tau$ . Based on the model in Section II, we know the autocorrelation of such a process is  $\varphi_{h,k} + \sigma_w^2 \delta_{k,0}$ , where  $\varphi_{h,k} = J_0(2\pi f_d T_s k)$  and  $J_0(\cdot)$  is the zeroth-order Bessel function of the first kind. Consequently,  $\sigma_P^2$  together with the linear predictor coefficients  $\mathbf{a}_P \triangleq [a_1, \dots, a_P]^T$  can be

solved from the Yule-Walker equations, i.e.

$$[P_R \Phi_{P+1} + \sigma_w^2 \mathbf{I}_{P+1}] \begin{bmatrix} -1 \\ \mathbf{a}_P \end{bmatrix} = \begin{bmatrix} -\sigma_P^2 \\ \mathbf{0} \end{bmatrix}, \quad (19)$$

where

$$\Phi_{P+1} \triangleq \begin{bmatrix} \varphi_{h,0} & \varphi_{h,-1} & \cdots & \varphi_{h,-P} \\ \varphi_{h,1} & \varphi_{h,0} & \cdots & \varphi_{h,-P+1} \\ \vdots & \vdots & \ddots & \vdots \\ \varphi_{h,P} & \cdots & \cdots & \varphi_{h,0} \end{bmatrix}.$$

If we denote

$$\varphi_P \triangleq \begin{bmatrix} \varphi_{h,1} \\ \vdots \\ \varphi_{h,P} \end{bmatrix},$$

after some manipulations we have (c.f. [42] (17))

$$\rho_{\text{eff}}(\rho) = \frac{\rho \varphi_P^H [\Phi_P + \rho^{-1} \mathbf{I}_P]^{-1} \varphi_P}{1 + \rho - \rho \varphi_P^H [\Phi_P + \rho^{-1} \mathbf{I}_P]^{-1} \varphi_P}. \quad (20)$$

The integral in (16) can be numerically evaluated by using the Gaussian quadrature rule with Chebyshev polynomials [46]. That is

$$\begin{aligned} P_{k,l}(\rho) &= \frac{1}{\pi} \int_0^1 \prod_{m=1}^{N_T} \left[ 1 + \frac{\rho_{\text{eff}}(\rho) \sigma_{m,k,l}^2}{4x^2} \right]^{-N_T} \frac{1}{\sqrt{1-x^2}} dx \\ &\approx \frac{1}{2\pi} \sum_{n=1}^{N_p} C_{x_n} \prod_{m=1}^{N_T} \left[ 1 + \frac{\rho_{\text{eff}}(\rho) \sigma_{m,k,l}^2}{4x_n^2} \right]^{-N_T}, \end{aligned} \quad (21)$$

where  $\{x_n\}_{n=1}^{N_p}$  are the roots of the  $N_p$ th-order Chebyshev polynomial and can be found in [46] together with the values of  $\{C_{x_n}\}_{n=1}^{N_p}$ . Furthermore, when a special class of  $2 \times 2$  DUSTM constellations [41] is considered, the integral in (16) can be expressed in closed-form as a finite sum [42].

The ESTT EI erases the demodulated symbol based on the threshold test (7), where  $\hat{\rho}_{\text{eff},\tau}$  is an estimate of  $\rho_{\text{eff}}(\rho)$ . Although this is equivalent to a threshold test on the received SIR with threshold  $\rho_{\text{th}} \triangleq \rho_{\text{eff}}^{-1}(\rho_{\text{eth}})$ , the latter is not straightforward for implementation because  $\rho$  is not easily estimated at the receiver. Nevertheless, the post-EI symbol error/erasure probabilities can

be expressed as

$$P_a(\rho, \rho_{\text{th}}) = \begin{cases} 1, & \rho \leq \rho_{\text{th}} \\ 0, & \rho > \rho_{\text{th}} \end{cases} \quad (22)$$

and

$$P_e(\rho, \rho_{\text{th}}) = \begin{cases} 0, & \rho \leq \rho_{\text{th}} \\ P_e(\rho), & \rho > \rho_{\text{th}} \end{cases} \quad (23)$$

for a certain threshold  $\rho_{\text{th}} > 0$ .

The analytic decoding error probability of ESTT EI based on (22) (23) is shown to be in good accuracy with the link simulation results in [13], where the EI rule (7) is used. Furthermore, another threshold-test EI rule is derived in [13] based on Bayesian decision framework [43]. In addition to achieving optimum performance, the Bayesian EI is robust to the choice of its threshold, which is critical for practical implementation. On the other hand, performance of ESTT is shown to be relatively sensitive to the choice of  $\rho_{\text{th}}$  but its analytic tractability is desired for network performance analysis. This apparent gap is bridged by results in [13], which showed that analysis of ESTT EI with optimized  $\rho_{\text{th}}$  predicts the performance of Bayesian EI accurately in interference dominated environment. This justifies the network analysis in this paper based on ESTT EI with optimized thresholds, which also sheds light on the expected performance when the Bayesian EI is used.

### B. Distribution of the MAI power

Due to the nature of Poisson processes on a plane, interfering nodes are uniformly distributed in a circle centered at  $\mathcal{D}$  with an arbitrary radius  $a$  [47]. That is, the pdf of  $d_k$  is given by

$$f_d(r) = \frac{2r}{a^2} \quad (r \leq a). \quad (24)$$

For a random vector  $\mathbf{Y}$  in the general form of  $\mathbf{Y} = \lim_{a \rightarrow \infty} \sum_k^{[\lambda' \pi a^2]} d_k^{-b} \mathbf{X}_k$  where  $\mathbf{X}_k$ s are i.i.d. random vectors and  $d_k$ s are i.i.d. with pdf in (24), its joint characteristic function (CF) is derived by Sousa [48] when  $\mathbf{X}_k$ s have zero-mean and finite second-order moment and by Ilow et al [49] [50] when  $\mathbf{X}_k$ s are spherically symmetric. However, results in [48] [49] [50] cannot be directly applied to obtain the CF of  $\sigma_w^2$  considered in this paper because the log-normal r.v.  $S_k$  in (10) is neither zero-mean nor spherically symmetric. In the following, we derive  $\phi_{\text{MAI}}(\omega)$ , the CF of

$\sigma_w^2$ , based on the influence function method [48] [51].

By definition, we can write  $\phi_{\text{MAI}}(\omega)$  since

$$\phi_{\text{MAI}}(\omega) = \mathbb{E} \left[ e^{j\omega\sigma_w^2} \right] = \lim_{a \rightarrow \infty} \mathbb{E} \left\{ e^{j\omega \sum_k^{\lfloor \lambda' \pi a^2 \rfloor} d_k^{-b} S_k} \right\}. \quad (25)$$

Since  $d_k, S_k$  are i.i.d. and the number of summands in (25) is a Poisson r.v., we have

$$\begin{aligned} \phi_{\text{MAI}}(\omega) &= \lim_{a \rightarrow \infty} \sum_{k=0}^{\infty} \frac{(\lambda' \pi a^2)^k e^{-\lambda' \pi a^2}}{k!} \left\{ \mathbb{E} \left[ \exp(j\omega d^{-b} S) \right] \right\}^k \\ &= \lim_{a \rightarrow \infty} \exp \left\{ \lambda' \pi a^2 \left[ \mathbb{E} \left( e^{j\omega d^{-b} S} \right) - 1 \right] \right\}, \end{aligned} \quad (26)$$

where the r.v.s  $d$  and  $S$  are distributed according to (24) and (2) respectively. By denoting the CF of  $S$  to be  $\phi_S(\cdot)$  and integrating by part, the expectation in (26) can be evaluated as

$$\begin{aligned} \mathbb{E} \left( e^{j\omega d^{-b} S} \right) &= \int \mathbb{E} \left[ e^{j\omega r^{-b} S} \right] \cdot f_d(r) dr \\ &= \int_0^a \phi_S(r^{-b} \omega) \frac{2r}{a^2} dr \\ &= \phi_S(a^{-b} \omega) - \lim_{r \rightarrow 0} \frac{r^2}{a^2} \phi_S(r^{-b} \omega) \\ &\quad - \int_0^a \frac{r^2}{a^2} \frac{d\phi_S(r^{-b} \omega)}{dr} dr. \end{aligned} \quad (27)$$

The second term in (27) is zero if  $\phi_S(\omega)$  is bounded for arbitrary  $\omega$ . Furthermore, by applying L'Hopital's rule, we have

$$\begin{aligned} \lim_{a \rightarrow \infty} \lambda' \pi a^2 \left[ \phi_S(a^{-b} \omega) - 1 \right] &= \lambda' \pi \lim_{x \rightarrow 0} \frac{\phi_S(x^b \omega) - 1}{x^2} \\ &= \frac{\lambda' \pi \omega}{2} \lim_{x \rightarrow 0} \phi_S'(x^b \omega) x^{b-2} \\ &= \frac{\lambda' \pi j \omega}{2} \mathbb{E}[S] \lim_{x \rightarrow 0} x^{b-2}. \end{aligned} \quad (28)$$

If we assume the path-loss exponent satisfies  $b > 2$ , then we have the following from (26) (27)

(28):

$$\begin{aligned}\phi_{\text{MAI}}(\omega) &= \exp\left(-\lambda'\pi \int_0^\infty r^2 \frac{d\phi_S(r^{-b}\omega)}{dr} dr\right) \\ &= \exp\left(\lambda'\pi \int_0^\infty \frac{d\phi_S(t\omega)}{dt} t^{-2/b} dt\right).\end{aligned}\quad (29)$$

The integral in (29) can be further simplified as

$$\begin{aligned}\int_0^\infty \frac{d\phi_S(t\omega)}{dt} t^{-\alpha} dt &= \int_0^\infty \mathbb{E}\left[\frac{d}{dt} e^{jSt\omega}\right] t^{-\alpha} dt \\ &= j\omega \mathbb{E}\left[S \int_0^\infty e^{jSt\omega} t^{-\alpha} dt\right] \\ &= j\omega \mathbb{E}\left[S \frac{\Gamma(1-\alpha)}{(-jS\omega)^{1-\alpha}}\right] \\ &= -\Gamma(1-\alpha) (-j\omega)^\alpha \mathbb{E}[S^\alpha],\end{aligned}\quad (30)$$

where  $\Gamma(x) = \int_0^\infty t^{x-1} e^{-t} dt$  is the Gamma function and  $(\cdot)^\alpha$  refers to the principle value, i.e.

$$(-j\omega)^\alpha = \begin{cases} e^{-j\alpha\pi/2} |\omega|^\alpha & \omega \geq 0 \\ e^{j\alpha\pi/2} |\omega|^\alpha & \omega < 0 \end{cases}.$$

Consequently, if we denote  $\alpha = 2/b$  and notice that  $\mathbb{E}[S^\alpha] = \exp\left(\alpha^2 \frac{\sigma_s^2}{2}\right)$  for log-normal r.v.  $S$ , the CF of  $\sigma_w^2$  for  $b > 2$  reduces to

$$\begin{aligned}\phi_{\text{MAI}}(\omega) &= \exp\left[-\lambda'\pi\Gamma(1-\alpha) e^{\frac{1}{2}\alpha^2\sigma_s^2} (-j\omega)^\alpha\right] \\ &= \exp\left[-\lambda'\pi\Gamma(1-\alpha) e^{\frac{1}{2}\alpha^2\sigma_s^2} \cos\frac{\alpha\pi}{2} |\omega|^\alpha \left(1 - j \operatorname{sgn}(\omega) \tan\frac{\alpha\pi}{2}\right)\right],\end{aligned}\quad (31)$$

from which it is clear that  $\sigma_w^2$  is an alpha-stable r.v. [52].

Unfortunately, the pdf of  $\sigma_w^2$  can be expressed in closed-form only when  $b = 4$ , in which case the alpha-stable distribution coincides with the Levy distribution and

$$\begin{aligned}\phi_{\text{MAI}}(\omega) &= \exp\left[-\lambda'\pi^{3/2} e^{\sigma_s^2/8} \sqrt{-j\omega}\right] \\ &\triangleq \exp\left[-\gamma \sqrt{-2j\omega}\right]\end{aligned}$$

with  $\gamma \triangleq \lambda\pi^{3/2} e^{\sigma_s^2/8} / \sqrt{2}$ . In this case the pdf and the cumulative distribution function (cdf) of

$\sigma_w^2$  when  $b = 4$  are available as

$$\begin{aligned} f_{\text{MAI}}(x) &= \frac{\gamma}{\sqrt{2\pi}} x^{-\frac{3}{2}} \exp\left(-\frac{\gamma^2}{2x}\right) \\ &= \frac{\lambda' \pi}{2} e^{\sigma_s^2/8} x^{-\frac{3}{2}} \exp\left(-\frac{\lambda'^2 \pi^3 e^{\sigma_s^2/4}}{4x}\right) \quad (x \geq 0), \\ F_{\text{MAI}}(x) &= \operatorname{erfc}\left(\frac{\gamma}{\sqrt{2x}}\right) = \operatorname{erfc}\left(\frac{\lambda' \pi^{3/2} e^{\sigma_s^2/8}}{2\sqrt{x}}\right) \quad (x \geq 0). \end{aligned}$$

We will focus on the ground wave propagation model ( $b = 4$ ) in the rest of the paper due to the analytic tractability.

### C. Decoding error probability

The decoding error probability in the presence of EI is given by [43]

$$P_C = \sum_{i=0}^L \sum_{j=j_0(i)}^{n-i} \frac{n!}{i!j!(n-i-j)!} \bar{P}_e^i \bar{P}_a^j (1 - \bar{P}_e - \bar{P}_a)^{n-i-j}. \quad (32)$$

where  $j_0(i) \triangleq \max(L-K+1-2i, 0)$  and  $\bar{P}_a, \bar{P}_e$  are the probabilities of symbols in a codeword being erased or erroneous, respectively. Alternatively, the decoding error probability of error-only decoding is given by

$$P_C' = \sum_{i > \lceil \frac{L-k}{2} \rceil}^L \binom{n}{i} \tilde{P}_e^i (1 - \tilde{P}_e)^{n-i}, \quad (33)$$

where  $\tilde{P}_e$  is the symbol error probability without EI. In principle, the probabilities  $\tilde{P}_e, \bar{P}_a, \bar{P}_e$  can be obtained by averaging (17), (22), (23) over the distribution of  $\rho$ , which is derived in the next for slow and fast shadowing model separately.

*1) Slow shadowing:* In slow shadowing, transmitted symbols corresponding to the same codeword experience the same realization of log-normal shadowing. Therefore, the symbol erasure/error probabilities and consequently the decoding error probability have to be derived by conditioning on the shadowing first. The average decoding error probability is then obtained by average over the log-normal distribution (2).

Based on (15) and conditioning on the shadowing  $S_0$ , it is easy to see that the pdf of received

SIR is given by

$$\begin{aligned} f_{\rho|S_0}(t) &= \frac{S_0}{t^2 R^b} f_{\text{MAI}}\left(\frac{S_0}{tR^b}\right) \\ &= \frac{N'_0 e^{\sigma_s^2/8}}{2\sqrt{S_0 t}} \exp\left(-\frac{N_0'^2 \pi e^{\sigma_s^2/4}}{4S_0} t\right), \end{aligned} \quad (34)$$

where

$$N'_0 \triangleq \lambda' \pi R^2 = \frac{p}{q} N_0. \quad (35)$$

Similarly, the conditional cdf of  $\rho$  is given by

$$\begin{aligned} F_{\rho|S_0}(t) &= 1 - F_{\text{MAI}}\left(\frac{S_0}{tR^b}\right) \\ &= \text{erf}\left(\frac{N'_0 e^{\sigma_s^2/8}}{2} \sqrt{\frac{\pi t}{S_0}}\right). \end{aligned} \quad (36)$$

By averaging (22) (23) over the distribution (34), we obtain the conditional symbol erasure/error probabilities as

$$\begin{aligned} \bar{P}_{a|S_0}(\rho_{\text{th}}) &= F_{\rho|S_0}(\rho_{\text{th}}) \\ &= \text{erf}\left(\frac{N'_0 e^{\sigma_s^2/8}}{2} \sqrt{\frac{\pi}{S_0} \rho_{\text{th}}}\right), \end{aligned} \quad (37)$$

$$\begin{aligned} \bar{P}_{e|S_0}(\rho_{\text{th}}) &= \int P_e(\rho, \rho_{\text{th}}) f_{\rho|S_0}(\rho) d\rho \\ &= \int_{\rho > \rho_{\text{th}}} \frac{N'_0 e^{\sigma_s^2/8}}{2\sqrt{S_0} \rho} \exp\left(-\frac{N_0'^2 \pi e^{\sigma_s^2/4}}{4S_0} \rho\right) P_e(\rho) d\rho. \end{aligned} \quad (38)$$

The integral in (38) can be numerically evaluated by Gaussian quadrature rule with Laguerre

polynomials [46] as following:

$$\begin{aligned}
\bar{P}_{e|S_0}(\rho_{\text{th}}) &= \int_0^\infty \frac{N'_0 \exp\left(\frac{\sigma_s^2}{8} - \frac{N_0'^2 \pi e^{\sigma_s^2/4}}{4S_0} \rho_{\text{th}}\right)}{2\sqrt{S_0}(\rho + \rho_{\text{th}})} \exp\left(-\frac{N_0'^2 \pi e^{\sigma_s^2/4}}{4S_0} \rho\right) P_e(\rho + \rho_{\text{th}}) d\rho \\
&= \frac{2\sqrt{S_0}}{N'_0 \pi} \exp\left(-\frac{\sigma_s^2}{8} - \frac{N_0'^2 \pi e^{\sigma_s^2/4}}{4S_0} \rho_{\text{th}}\right) \\
&\quad \times \int_0^\infty e^{-\rho} \cdot \left[\frac{4S_0}{N_0'^2 \pi e^{\sigma_s^2/4}} \rho + \rho_{\text{th}}\right]^{-\frac{1}{2}} P_e\left(\frac{4S_0}{N_0'^2 \pi e^{\sigma_s^2/4}} \rho + \rho_{\text{th}}\right) d\rho \\
&\cong \frac{2\sqrt{S_0}}{N'_0 \pi} \exp\left(-\frac{\sigma_s^2}{8} - \frac{N_0'^2 \pi e^{\sigma_s^2/4}}{4S_0} \rho_{\text{th}}\right) \sum_{m=1}^{N_p} L_{y_m} \cdot \left[\rho^{-\frac{1}{2}} P_e(\rho)\right]_{\rho=\frac{4S_0 y_m}{N_0'^2 \pi e^{\sigma_s^2/4}} + \rho_{\text{th}}} . \quad (39)
\end{aligned}$$

where  $\{y_m\}_{m=1}^{N_p}$  are the roots of the  $N_p$ -th-order Laguerre polynomial and can be found in [46] together with the values of  $\{L_{y_m}\}_{m=1}^{N_p}$ . The decoding error probability conditioned on  $S_0$  is given by

$$\begin{aligned}
P_{C|S_0}(\rho_{\text{th}}) &= \sum_{i=0}^{n_c} \sum_{j=j_0(i)}^{n_c-i} \frac{n_c!}{i!j!(n_c-i-j)!} \bar{P}_{e|S_0}^i(\rho_{\text{th}}) \bar{P}_{a|S_0}^j(\rho_{\text{th}}) \\
&\quad \times [1 - \bar{P}_{e|S_0}(\rho_{\text{th}}) - \bar{P}_{a|S_0}(\rho_{\text{th}})]^{n_c-i-j} \quad (40)
\end{aligned}$$

Optimizing over  $\rho_{\text{th}}$  (the optimal  $\rho_{\text{th}}$  depends on the realization of  $S_0$ ), we get

$$P_{C|S_0} = \min_{\rho_{\text{th}}} P_{C|S_0}(\rho_{\text{th}}). \quad (41)$$

The decoding error probability is then obtained by averaging over the log-normal distribution of  $S_0$ :

$$\begin{aligned}
P_C &= E_{S_0} [P_{C|S_0}] = \int_{-\infty}^{\infty} \frac{1}{\sqrt{2\pi}\sigma_s} e^{-\frac{z^2}{2\sigma_s^2}} P_{C|e^z} dz \\
&= \frac{1}{\sqrt{\pi}} \int_{-\infty}^{\infty} e^{-z^2} P_{C|e^{\sqrt{2}\sigma_s z}} dz . \quad (42)
\end{aligned}$$

The integral in (42) can be numerically evaluated by applying Gaussian quadrature rule with Hermite polynomials [46]. That is,

$$P_C \cong \frac{1}{\sqrt{\pi}} \sum_{n=1}^{N_p} H_{x_n} P_{C|e^{\sqrt{2}\sigma_s x_n}} \quad (43)$$

where  $\{x_n\}_{n=1}^{N_p}$  are the roots of the  $N_p$ th-order Hermite polynomial and can be found in [46] together with the values of  $\{H_{x_n}\}_{n=1}^{N_p}$ . Similarly, the decoding error probability without EI is given by

$$\begin{aligned} P'_C &= E_{S_0} [P'_{C|S_0}] \\ &= \frac{1}{\sqrt{\pi}} \int_{-\infty}^{\infty} e^{-z^2} P'_{C|e^{\sqrt{2}\sigma_s z}} dz \\ &\cong \frac{1}{\sqrt{\pi}} \sum_{n=1}^{N_p} H_{x_n} P'_{C|e^{\sqrt{2}\sigma_s x_n}} \end{aligned} \quad (44)$$

where  $P'_{C|S_0}$  is given by (33) with  $\tilde{P}_e$  substituted by  $\bar{P}_{e|S_0}(0)$  (c.f. (38) (39)).

2) *Fast shadowing*: In fast shadowing, different dwells are assumed to be subject to independent shadowing realizations. Consequently, the SIR in a given dwell has a pdf given by  $f_\rho(t) = E_{S_0} [f_{\rho|S_0}(t)]$  where  $f_{\rho|S_0}(t)$  is given in (34). By applying Gaussian quadrature rule with Hermite polynomials again, we have

$$\begin{aligned} f_\rho(t) &= \int_{-\infty}^{\infty} \frac{1}{\sqrt{2\pi}\sigma_s} e^{-\frac{x^2}{2\sigma_s^2}} f_{\rho|e^x}(t) dx \\ &= \frac{N'_0 e^{\sigma_s^2/4}}{2\sqrt{\pi t}} \int_{-\infty}^{\infty} e^{-y^2} \exp\left(-\frac{N_0'^2 \pi e^{3\sigma_s^2/4}}{4} e^{-\sqrt{2}\sigma_s y t}\right) dy \\ &\cong \frac{N'_0 e^{\sigma_s^2/4}}{2\sqrt{\pi t}} \sum_{n=1}^{N_p} H_{x_n} \exp\left(-\frac{\pi}{4} N_0'^2 e^{3\sigma_s^2/4 - \sqrt{2}\sigma_s x_n} t\right), \end{aligned} \quad (45)$$

Based on (45), the symbol erasure probability is given by

$$\begin{aligned} \bar{P}_a(\rho_{\text{th}}) &= \int_0^{\rho_{\text{th}}} f_\rho(t) dt \\ &\cong \frac{N'_0 e^{\sigma_s^2/4}}{2\sqrt{\pi}} \sum_{n=1}^{N_p} H_{x_n} \int_0^{\rho_{\text{th}}} t^{-1/2} \exp\left(-\frac{\pi}{4} N_0'^2 e^{3\sigma_s^2/4 - \sqrt{2}\sigma_s x_n} t\right) dt \\ &= \frac{e^{-\sigma_s^2/8}}{\sqrt{\pi}} \sum_{n=1}^{N_p} H_{x_n} e^{\sigma_s x_n / \sqrt{2}} \operatorname{erf}\left(\frac{N'_0}{2} e^{3\sigma_s^2/8 - \sigma_s x_n / \sqrt{2}} \sqrt{\pi \rho_{\text{th}}}\right), \end{aligned} \quad (46)$$

where we have applied  $\int_0^\rho t^{-1/2} e^{-bt} dt = \sqrt{\frac{\pi}{b}} \operatorname{erf}(\sqrt{b\rho})$ . The post-EI symbol error probability is

then

$$\begin{aligned}\bar{P}_e(\rho_{\text{th}}) &= \int_{\rho > \rho_{\text{th}}} P_e(\rho) f_\rho(\rho) d\rho \\ &\cong \frac{N'_0 e^{\sigma_s^2/4}}{2\sqrt{\pi}} \sum_{n=1}^{N_p} H_{x_n} \int_{\rho > \rho_{\text{th}}} \frac{P_e(\rho)}{\sqrt{\rho}} \exp\left(-\frac{\pi N_0'^2}{4} e^{\frac{3}{4}\sigma_s^2 - \sqrt{2}\sigma_s x_n} \rho\right) d\rho, \quad (47)\end{aligned}$$

where the integral can be further evaluated by Gaussian quadrature rule with Laguerre polynomials [46]. If we denote  $c \triangleq \frac{4}{\pi N_0'^2} e^{-3\sigma_s^2/4}$  and change variables, we have

$$\begin{aligned}&\int_{\rho > \rho_{\text{th}}} \frac{P_e(\rho)}{\sqrt{\rho}} \exp\left(-\frac{\pi N_0'^2}{4} e^{\frac{3}{4}\sigma_s^2 - \sqrt{2}\sigma_s x_n} \rho\right) d\rho \\ &= c \exp\left(-\frac{\rho_{\text{th}}}{ce^{\sqrt{2}\sigma_s x_n}}\right) e^{\sqrt{2}\sigma_s x_n} \int_0^\infty \frac{P_e\left(ce^{\sqrt{2}\sigma_s x_n} \rho + \rho_{\text{th}}\right)}{\sqrt{ce^{\sqrt{2}\sigma_s x_n} \rho + \rho_{\text{th}}}} e^{-\rho} d\rho \\ &\cong c \exp\left(\sqrt{2}\sigma_s x_n - \frac{\rho_{\text{th}}}{ce^{\sqrt{2}\sigma_s x_n}}\right) \sum_{m=1}^{N'_p} L_{y_m} \frac{P_e\left(ce^{\sqrt{2}\sigma_s x_n} y_m + \rho_{\text{th}}\right)}{\sqrt{ce^{\sqrt{2}\sigma_s x_n} y_m + \rho_{\text{th}}}}, \quad (48)\end{aligned}$$

and consequently

$$\bar{P}_e(\rho_{\text{th}}) \cong \frac{2e^{-\sigma_s^2/2}}{\pi^{3/2} N_0'} \sum_{n=1}^{N_p} H_{x_n} \exp\left(\sqrt{2}\sigma_s x_n - \frac{\rho_{\text{th}}}{ce^{\sqrt{2}\sigma_s x_n}}\right) \sum_{m=1}^{N'_p} L_{y_m} \frac{P_e\left(ce^{\sqrt{2}\sigma_s x_n} y_m + \rho_{\text{th}}\right)}{\sqrt{ce^{\sqrt{2}\sigma_s x_n} y_m + \rho_{\text{th}}}}. \quad (49)$$

The decoding error probability is again given by (32) and, after optimizing over the threshold, we have

$$P_C = \min_{\rho_{\text{th}}} P_C(\rho_{\text{th}}). \quad (50)$$

The error-only decoding error probability  $P'_C$  is given by (33) with  $\tilde{P}_e$  substituted by  $\bar{P}_e(0)$  (c.f. (49)).

#### D. Optimizing IE

To express the results in dimensionless quantities, we multiply the IE defined in (12) by  $\sqrt{\lambda}$  and obtain

$$\sqrt{\lambda} IE = \frac{1}{\sqrt{\pi}} \tau(p) \cdot (1 - P_C) \cdot \xi \cdot \sqrt{N_0}. \quad (51)$$

The transmission range  $R$  is equivalently specified by  $N_0 = \lambda\pi R^2$ . The (normalized) IE depends on various factors, including the transmitted waveform (spreading gain  $q$ , number of transmit antennas  $N_T$ , DUSTM constellation, RS code parameters  $L, K$ ), the receiver configuration (the feedback length  $P$ , number of receive antenna  $N_R$ , with or without EI), the MAC (the ALOHA transmission probability  $p$ ), and the channel statistics (path-loss exponent, normalized Doppler frequency  $f_d T_s$ , shadowing spread  $\sigma_s$  and shadowing coherence time). The focus of this paper is to study the trade-off between  $\sqrt{\lambda}IE$  and  $N_0$ , and also investigate the impact of various system parameters and channel statistics on such trade-off.

From the analysis in Section III-C, we notice that the decoding error probability depends on  $N'_0 = \frac{p}{q}N_0$ . Therefore, we can write

$$\begin{aligned}\sqrt{\lambda}IE &= \frac{\tau(p)}{\sqrt{\pi p}} \sqrt{q\xi} \cdot [1 - P_C(N'_0)] \sqrt{N'_0} \\ &= \frac{\tau(p)}{\sqrt{\pi p}} \frac{\log_2(L)}{\sqrt{q}} \frac{K}{L} [1 - P_C(N'_0)] \sqrt{N'_0}.\end{aligned}\quad (52)$$

It is clear that the optimal transmission probability in the slotted-ALOHA MAC is given by

$$p_{\text{opt}} = \arg \max_p \sqrt{\lambda}IE = \arg \max_p \frac{\tau(p)}{\sqrt{\pi p}} = 0.27$$

which is the same as the value obtained in [27] [34]. Substituting  $p_{\text{opt}}$  into (52) we have

$$\sqrt{\lambda}IE = 0.0975 \frac{\log_2(L)}{\sqrt{q}} \frac{K}{L} [1 - P_C(N'_0)] \sqrt{N'_0}\quad (53)$$

where

$$N'_0 = 0.27 \frac{N_0}{q}.\quad (54)$$

The role of spreading gain  $q$  can be readily observed from (53) and (54). Specifically, when other parameters are fixed in (53), the maximum achievable IE by optimizing  $N_0$  is inversely proportional to  $\sqrt{q}$ , while the optimal  $N_0$  is proportional to  $q$  due to (54). In other words, the transmission range can be extended by increasing the spreading gain to reduce the effective MAI. However, the IE of the network is on the same order as  $q^{-\frac{1}{2}}$  according to (53) because the spectral efficiency is on the order of  $\frac{1}{q}$ , which outweighs the transmission range extension on the order of  $\sqrt{q}$ . Therefore, it is useful to study the trade-off between  $\sqrt{\lambda}IE$  and  $\frac{N_0}{q}$ . Since  $N_0$  is the expected number of nodes closer to  $\mathcal{D}$  than  $\mathcal{S}$ , we will refer to  $\frac{N_0}{q}$  by the *expected*

number of in-range nodes per bandwidth. Once the value of (c.f. (54))

$$\left(\frac{N_0}{q}\right)^{\text{opt}} = \frac{1}{0.27} \arg \max_{N'_0} [1 - P_C(N'_0)] \sqrt{N'_0} \quad (55)$$

and the corresponding IE are found for a given value of  $q$ , the optimal transmission range and maximum IE can be easily found by scaling for a network with the same setting except a different spreading gain. Specifically, the optimum  $N_0$  scales linearly with the spreading gain  $q$  according to (55) and the gradient of  $N_0^{\text{opt}}$  depends on channel statistics and the transceiver. This is in contrast with the results obtained by Sousa and Silvester [27] for DS-CDMA networks with single-user receiver, which showed that the optimum  $N_0$  is proportional to the square-root of the spreading gain. The corresponding IE is therefore on the order of  $\frac{1}{q} \cdot q^{\frac{1}{4}} = q^{-\frac{3}{4}} < q^{-\frac{1}{2}}$ . This may suggest the advantage of FH-CDMA over DS-CDMA in terms of both the transmission range and the IE, when the total bandwidth constraint is the same for both access schemes. Such an advantage comes from the better near-far resistance of FH-CDMA waveform compared to DS-CDMA with single-user receiver.

#### IV. NUMERICAL RESULTS

In this section, the trade-off between  $\sqrt{\lambda IE}$  and  $\frac{N_0}{q}$  and the impact of various parameters on such trade-off are studied in more details. The optimal ALOHA transmission probability  $p_{\text{opt}} = 0.27$  is always assumed. We also set  $q = 512$ , but as discussed in Section III-D, the results are easily interpreted for other values of  $q$ . Two transmit antennas are considered in simulation and the DUSTM constellations proposed in [41] are employed.

In Fig.4, curves of  $\sqrt{\lambda IE}$  versus  $\frac{N_0}{q}$  are plotted for DUSTM constellation size 4 and 64 with RS code rate  $\frac{1}{4}, \frac{1}{2}, \frac{3}{4}$ , respectively. Two received antennas are used with ESTT EI and the DFD feedback length  $P = 1$ , while fast shadowing model is considered with shadowing spread  $\sigma_s = 4.3\text{dB}$  and the normalized Doppler frequency is  $f_d T_s = 0.05$ . It is observed in Fig.4 that the MCS impacts the trade-off between IE and transmission range significantly. Specifically, lower code rate or smaller constellation size implies better error protection of the communication link, which leads to larger optimum transmission range but lower spectral efficiency. The latter apparently outweighs the former and we observe lower maximum IE as the code rate or constellation size decreases.

The dependence of IE and transmission range on MCS is illustrated more pronouncedly in Fig.5, where the optimum expected number of in-range nodes per bandwidth (c.f. (55)) and the corresponding maximum IE are shown for various MCSs by assuming ESTT EI and  $N_R = 2, P = 1, f_d T_s = 0.05$ . It is thus clear that the optimal MCS to maximize the best achievable IE depends on the desired transmission range. Furthermore, Fig.5 shows that the optimal MCS also depends on the channel quality and receiver configuration. For example, the achievable performance with constellation size 16 is uniformly better than with constellation size 64. Also in the latter case increasing code rate beyond a certain point may reduce both the maximum IE and the optimal transmission range. Therefore, it is important to select the MCS that may be well supported by the channel quality and receiver configuration.

The next two figures (Fig.6,7) shows the effects of different channels on the IE and optimal transmission range. ESTT EI and  $N_R = 2, L = 16, K = 4$  are used in both figures. Curves in Fig.6 correspond to different shadowing models with the same mobility  $f_d T_s = 0.05$  and  $P = 1$ . The maximum achievable IE is higher for fast shadowing model than for slow shadowing model because higher time diversity is available when symbols in the same codeword are subject to independent shadowing. However, the corresponding values of  $\left(\frac{N_0}{q}\right)^{\text{opt}}$  under the two models are only slightly different. On the other hand, as the MAI becomes more dominant, slow shadowing leads to higher IE because some codewords may be successfully decoded when the corresponding shadowing gains are large, while their decoding may all fail in fast shadowing if the average shadowing gain is not adequate to support the high interference level. Translated in terms of dwell length, this indicates that whether long or short dwell is advantageous depends on the transmission range among other factors. As expected, the gap between the fast and slow shadowing model is reduced as  $\sigma_s$  decreases and the shadowing becomes more deterministic.

The effect of different mobility is shown in Fig.7. Higher mobility results in lower maximum achievable IE and nearer optimum transmission range, as can be seen by comparing the three curves corresponding to  $P = 1$  and  $f_d T_s = 0.01, 0.05, 0.1$ , respectively. However, the performance may be significantly improved by increasing the DFD feedback length  $P$ . For example, the curve for  $f_d T_s = 0.1$  and  $P = 5$  is close to the curves for lower mobility and  $P = 1$ , when the feedback is assumed error-free. In addition to the feedback length  $P$ , it is shown in Fig.8 that the spatial diversity from receive antenna array and interference suppression capability from EI are very valuable for improving the network performance, which corroborate their importance

in the link performance reported in [13] [14].

## V. CONCLUSION

In this paper, information efficiency and transmission range optimization is studied for mobile ad hoc networks with nodes accessing the channel by FH-CDMA and slotted-ALOHA. MIMO transceiver model proposed in [13] [14] is considered, where Reed-Solomon codes and differential unitary space-time modulation are employed with decision-feedback demodulation and erasure insertion decoding. The time-varying channel between any two nodes is subject to path-loss, log-normal shadowing, and Rayleigh fading. Effects of different Doppler frequency shifts due to mobility and different time-scale of shadowing variation revealed in this paper are not available in previous literature.

We have proved that the number of nodes in the optimum transmission range is proportional to the spreading gain in FH-CDMA networks, which implies higher information efficiency and further transmission range than DS-CDMA networks at large spreading gain [27]. It is also shown that the optimum transmission range and the corresponding information efficiency critically depend on the modulation and coding scheme. To maximize the achievable information efficiency, the modulation and coding scheme should be selected according to not only the target transmission range but also the channel condition and receiver setting. Significant improvement in network performance is observed with higher spatial diversity order and/or erasure insertion decoding, while increasing feedback length is shown to be effective in high mobility.

## REFERENCES

- [1] M. B. Pursley, "Frequency-hop transmission for satellite packet switching and terrestrial packet radio networks," *IEEE Trans. Info. Theory*, Vol.32, No.5, pp.652-667, Sep 1986
- [2] A. Ephremides, J. E. Wieselthier, D. J. Baker, "A design concept for reliable mobile radio networks with frequency hopping signaling," *Proc. of the IEEE*, Vol.75, No.1, pp.56-73, Jan. 1987
- [3] N. Kong, L. B. Milstein, "Error probability of multicell CDMA over frequency selective fading channels with power control error," *IEEE Trans. Commun.*, Vol.47, No.4, pp.608-617, April 1999
- [4] J. M. Romero-Jerez, C. Tellez-Labao, A. Diaz-Estrella, "Effect of power control imperfections on the reverse link of cellular CDMA networks under multipath fading," *IEEE Trans. Vehicular Tech.*, Vol.53, No.1, pp.61-71, Jan. 2004
- [5] P. Patel, J Holtzman, "Analysis of a simple successive interference cancellation scheme in a DS/CDMA system," *IEEE J. on Selected Areas of Commun.*, Vol.12, No.5, pp.796-807, Jun. 1994
- [6] U. Madhow, "Blind Adaptive Interference Suppression for Direct-Sequence CDMA," *Proc. of the IEEE*, Oct. 1998

- [7] S. Sfar, R. D. Murch, K. B. Letaief, "Layered space-time multiuser detection over wireless uplink systems," *IEEE Trans. Wireless Commun.*, Vol.2, No.4, pp.653-668, Jul. 2003
- [8] M. Pursley and D. Taipale, "Error probabilities for spread-spectrum packet radio with convolutional codes and Viterbi decoding," *IEEE Trans. Commun.*, Vol.35, No.1, pp.1-12, Jan. 1987
- [9] D. J. Torrieri, "Future army mobile multiple-access communications," *Proc. of IEEE Military Commun. Conf. (MILCOM)*, vol.2, pp.650-654, Nov. 1997
- [10] J. H. Gass, M. B. Pursley, "A comparison of slow-frequency-hop and direct-sequence spread-spectrum communications over frequency-selective fading channels," *IEEE Trans. Commun.*, Vol.47, No.5, pp.732-741, May 1999
- [11] J. H. Gass, M. B. Pursley, "A comparison of slow-frequency-hop and direct-sequence spread-spectrum packet communications over doubly selective fading channels," *IEEE Trans. Commun.*, Vol.50, No.8, pp.1236-1239, Aug. 2002
- [12] S. P. Weber, X. Yang, J. G. Andrews, G. de Veciana, "Transmission capacity of wireless ad hoc networks with outage constraints," *IEEE Trans. Info. Theory*, Vol.51, No.12, pp.4091-4102, Dec. 2005
- [13] H. Sui, J. R. Zeidler, "A robust coded MIMO FH-CDMA transceiver for mobile ad hoc networks," *IEEE J. on Selected Areas of Commun. (special issue on Optimization of MIMO Transceivers for Realistic Communication Networks)*, to be published in the 3rd quarter of 2007
- [14] H. Sui, J. R. Zeidler, "Erasure insertion for coded DUSTM-FHSS systems without a priori knowledge," *Proc. of IEEE Int. Conf. on Commun. (ICC)*, Vol.11, pp.5040-5046, June 2006
- [15] M. Park, S.-H. Choi, S. M. Nettles, "Cross-layer MAC design for wireless networks using MIMO," *Proc. IEEE Global Telecommun. Conf. (GLOBECOM)*, Vol.5, pp.2870-4, Nov. 2005
- [16] K. Sundaresan, R. Sivakumar, M. A. Ingram, T.-Y. Chang, "Medium access control in ad hoc networks with MIMO links: optimization consideration and algorithms," *IEEE Trans. Mobile Computing*, Vol.3, No.4, pp.350-365, Oct.-Dec. 2004
- [17] T. Tang, M. Park, R. W. Heath Jr., S. M. Nettles, "A joint MIMO-OFDM transceiver and MAC design for mobile ad hoc networking," *Int. Workshop on Wireless Ad Hoc Networks*, pp.315-9, May 2004
- [18] P. Casari, M. Levorato, M. Zorzi, "On the implications of layered space-time multiuser detection on the design of MAC protocols for ad hoc networks," *Proc. IEEE 16th Int. Symposium on Personal, Indoor and Mobile Radio Commun. (PIMRC)*, Vol.2, pp.1354-1360, Sept. 2005
- [19] J. C. Mundarath, P. Ramanathan, B. D. Van Veen, "NULLHOC: a MAC protocol for adaptive antenna array based wireless ad hoc networks in multipath environments," *Proc. IEEE Global Telecommun. Conf. (GLOBECOM)*, Vol.5, pp.2765-9, Nov. 2004
- [20] J.-S. Park, A. Nandan, M. Gerla, H. Lee, "SPACE-MAC: enabling spatial reuse using MIMO channel-aware MAC," *Proc. IEEE Int. Conf. on Commun. (ICC)*, Vol.5, pp.3642-6, May 2005
- [21] M. Zorzi, J. R. Zeidler, A. Anderson, B. Rao, J. Proakis, A. L. Swindlehurst, M. Jensen, S. Krishnamurthy, "Cross-layer issues in MAC protocol design for MIMO ad hoc networks," *IEEE Wireless Commun.*, Vol.13, No.4, pp.62-76, Aug. 2006
- [22] L. Kleinrock, J. A. Silvester, "Optimum transmission radii in packet radio networks or why six is a magic number," *Proc. Nat. Telecommunications Conf*, pp. 04.3.1-04.3.5, Birmingham, AL, Dec.1978
- [23] B. Hajek, "Adaptive transmission strategies and routing in mobile radio networks," *Proc. Conf. Info. Sci. Syst. (CISS)*, pp. 373-378, Mar. 1983.
- [24] H. Takagi, L. Kleinrock, "Optimal transmission ranges for randomly distributed packet radio networks," *IEEE Trans. Commun.*, Vol.32, No.3, pp.246-257, Mar. 1984.

- [25] T-C. Hou, V. O. K. Li, "Transmission range control in multihop packet radio networks," *IEEE Trans. Commun.*, Vol.34, No.2, pp.38-44, Jan. 1986
- [26] L. Kleinrock, J. A. Silvester, "Spatial reuse in multihop packet radio networks," *Proc. of the IEEE*, Vol.75, No.1, pp.156-167, Jan. 1987
- [27] E. S. Sousa, J. A. Silvester, "Optimum transmission ranges in a direct-sequence spread-spectrum multihop packet radio network," *IEEE J. on Selected Areas of Commun.*, Vol.8, No.5, pp.762-771, Jun. 1990
- [28] M. Zorzi, S. Pupolin, "Outage probability in multiple access packet radio networks in the presence of fading," *IEEE Trans. Vehicular Tech.*, Vol.43, No.3, pp.604-610, Aug. 1994
- [29] M. Zorzi, S. Pupolin, "Optimum transmission ranges in multihop packet radio networks in the presence of fading," *IEEE Trans. Commun.*, Vol.43, No.7, pp.2201-2205, July 1995
- [30] M. W. Chandra, B. L. Hughes, "Optimizing information efficiency in a direct-sequence mobile packet radio network," *IEEE Trans. Commun.*, Vol.51, No.1, pp.22-24, Jan. 2003
- [31] M. R. Souryal, B. R. Vojcic, R. L. Pickholtz, "Information efficiency of multihop packet radio networks with channel-adaptive routing," *IEEE J. on Selected Areas of Commun.*, Vol.23, No.1, pp.40-50, Jan. 2005
- [32] M. R. Souryal, B. R. Vojcic, R. L. Pickholtz, "Adaptive modulation in ad hoc DS/CDMA packet radio networks," *IEEE Trans. Commun.*, Vol.54, No.4, pp.714-725, Apr. 2006
- [33] M. W. Subbarao, B. L. Hughes, "Optimum transmission ranges in multihop packet radio networks in the presence of fading," *Proc. Conf. Info. Sci. and Systems (CISS)*, pp.684-689, Mar. 1997
- [34] M. W. Subbarao, B. L. Hughes, "Optimal transmission ranges and code rates for frequency-hop packet radio networks," *IEEE Trans. Commun.*, Vol.48, No.4, pp.670-678, Apr. 2000
- [35] P. C.P. Liang, W. E. Stark, "Transmission range control and information efficiency for FH packet radio networks," *Proc. of IEEE Military Commun. Conf. (MILCOM)*, Vol.2, pp.861-865, Oct. 2000
- [36] K. Stamatiou, J. G. Proakis, J. R. Zeidler, "Information efficiency of ad hoc networks with FH-MIMO transceivers," submitted to *IEEE Int. Conf. on Commun. (ICC)*, Jun. 2007
- [37] E. S. Sousa, J. A. Silvester, "Spreading code protocols for distributed spread-spectrum packet radio networks," *IEEE Trans. Commun.*, Vol.36, No.3, pp.272-81, Mar. 1988
- [38] A. Muqattash, M. Krunk, "CDMA-based MAC protocol for wireless ad hoc networks" *Proc. of 4th ACM Int. Symposium on Mobile Ad Hoc Networking & Computing (MOBIHOC)*, pp.153-164, June 2003
- [39] B. M. Hochwald, W. Sweldens, "Differential unitary space-time modulation," *IEEE Trans. Commun.*, Vol.48, No.12, pp.2041-2052, Dec. 2000
- [40] A. Shokrollahi, B. Hassibi, B. M. Hochwald, W. Sweldens, "Representation theory for high-rate multiple-antenna code design," *IEEE Trans. Info. Theory*, Vol.47, No.6, pp.2335-67, Setp. 2001
- [41] V. Tarokh, H. Jafarkhani, "A differential detection scheme for transmit diversity," *IEEE J. Selected Areas Commun.*, Vol.18, No.7, pp. 1169-74, July 2000
- [42] H. Sui, J. R. Zeidler, "An explicit and unified error probability analysis of two detection schemes for differential unitary space-time modulation," *Conf. Record of 39th Asilomar Conf. on Signals, Systems and Computer*, pp.1579-1583, Oct. 2005
- [43] C. W. Baum, M. B. Pursley, "Bayesian methods for erasure insertion in frequency-hop communications with partial-band interference," *IEEE Trans. Commun.*, Vol.40, No.7, pp. 1231-8, July 1992
- [44] J.-P. Linnartz, "Narrowband land-mobile radio networks," Artech House, Inc. 1993
- [45] William C. Jakes, Ed., "Microwave Mobile Communications," New York: John Wiley & Sons Inc., 1975

- [46] M. Abramowitz, I. A. Stegun, *Handbook of Mathematical Functions with Formulas, Graphs, and Mathematical Tables*, New York: Dover Publications, 1970
- [47] M. G. Kendall, P. A. P. Moran, *Geometrical Probability*, London, England: Griffin, 1963
- [48] E. S. Sousa, "Performance of a spread spectrum packet radio network link in a Poisson field of interferers," *IEEE Trans. Info. Theory*, Vol.38, No.6, pp.1743-1754, Nov. 1992
- [49] J. Ilow, D. Hatzinakos, "Analytic alpha-stable noise modeling in a Poisson field of Interferers or scatterers," *IEEE Trans. Sig. Proc.*, Vol.46, No.6, pp.1601-1611, June 1998
- [50] J. Ilow, D. Hatzinakos, A. N. Venetsanopoulos, "Performance of FH SS radio networks with interference modeled as a mixture of Gaussian and alpha-stable noise," *IEEE Trans. Commun.*, Vol.46, No.4, pp.509-520, Apr. 1998
- [51] V. M. Zolotarev, *One-dimensional stable distributions*, (translations of mathematical monographs), Providence, RI: American Mathematical Society, 1986, vol.65
- [52] M. Shao, C. L. Nikias, "Signal processing with fractional lower order moments: stable processes and their applications", *Proc. of the IEEE*, Vol.81, No.7, pp.986-1010, Jul. 1993

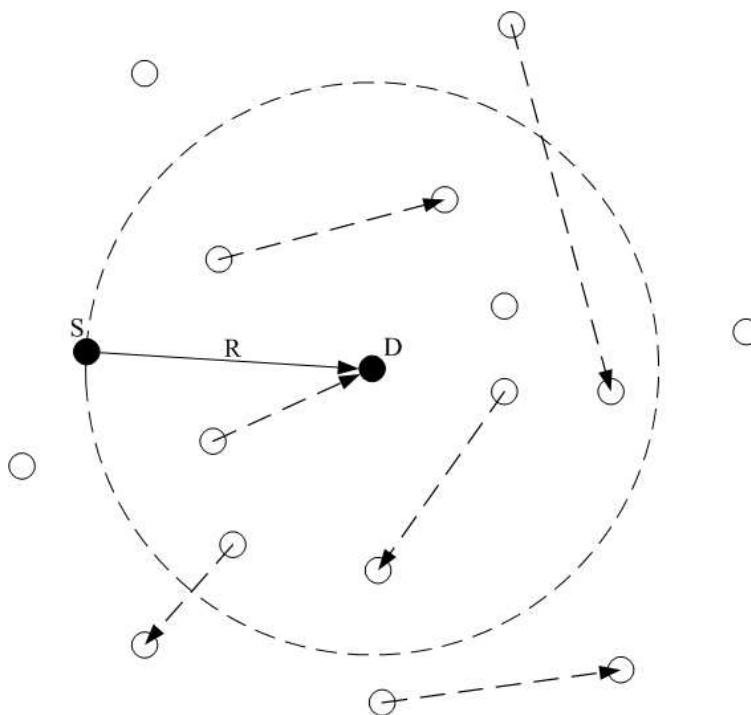


Fig. 1. Network model

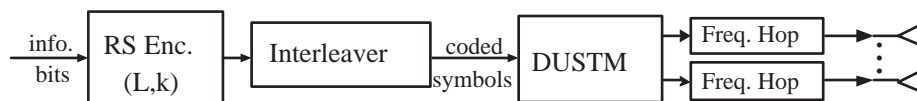


Fig. 2. Transmitter model

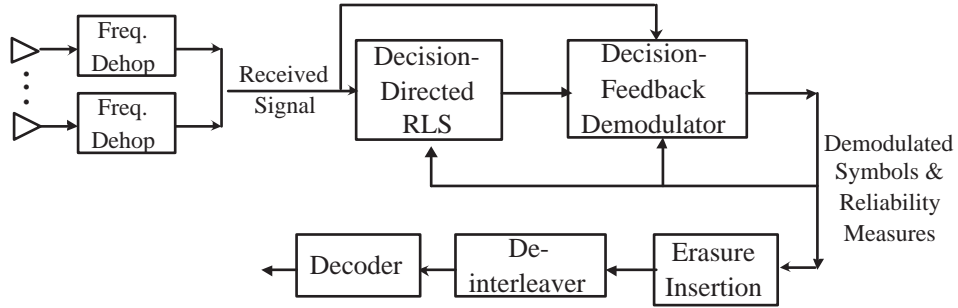


Fig. 3. Receiver model

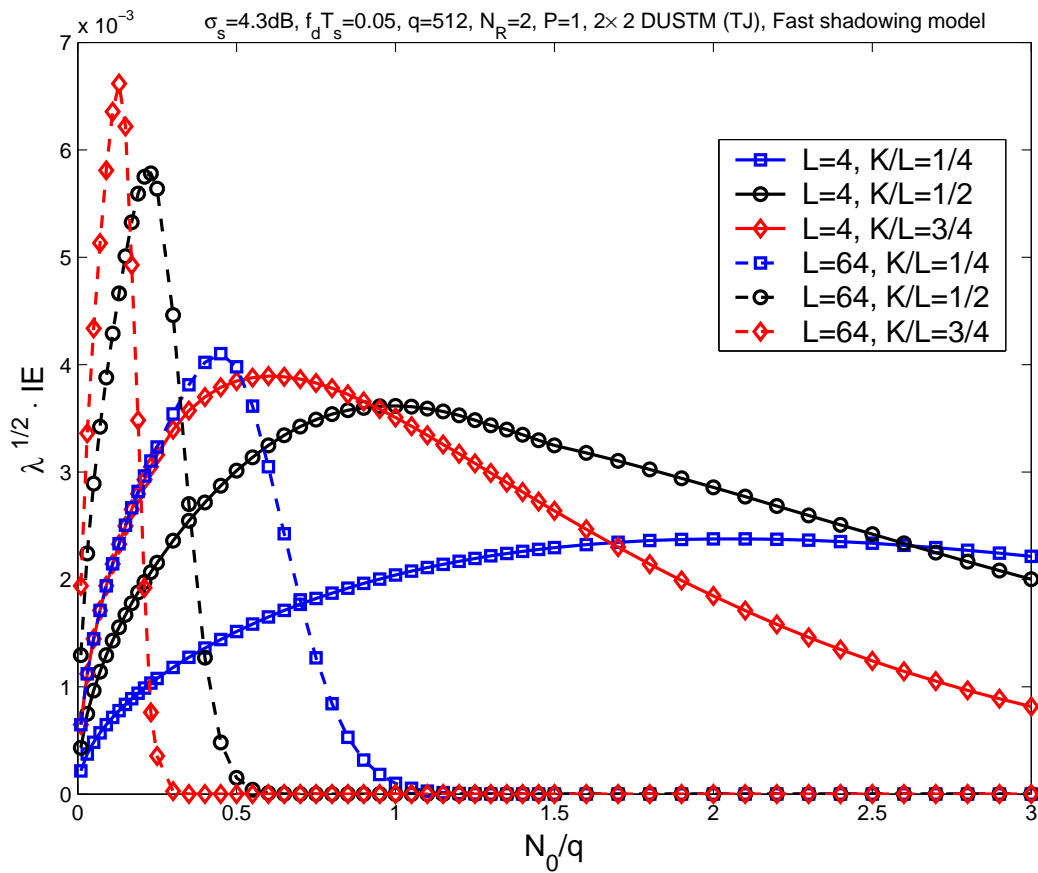


Fig. 4.  $\sqrt{\lambda}IE$  versus the expected number of in-range nodes per bandwidth  $\frac{N_0}{q}$  for different constellation sizes and code rates (two receive antennas, DFD feedback length  $P = 1$ , ESTT EI, shadowing spread  $\sigma_s = 4.3\text{dB}$ , fast shadowing model, normalized Doppler frequency  $f_d T_s = 0.05$ )

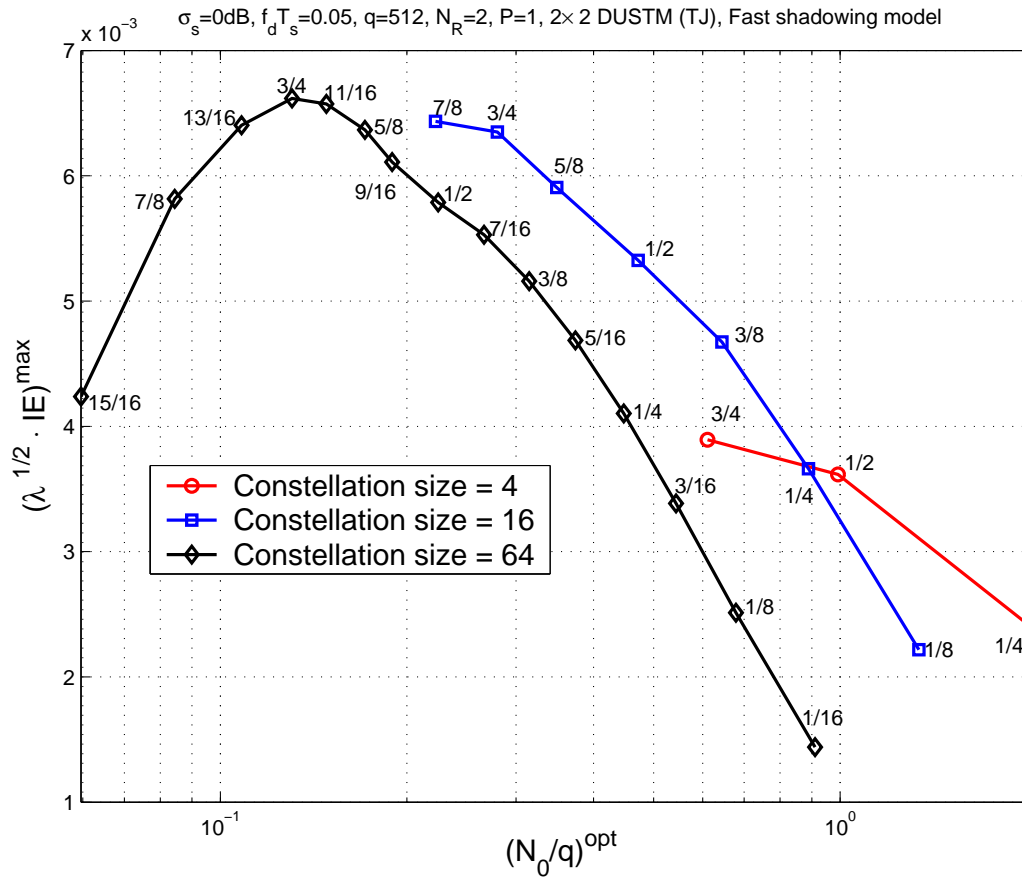


Fig. 5. Maximum IE  $(\sqrt{\lambda}IE)^{\text{max}}$  and optimum expected number of in-range nodes per bandwidth  $(\frac{N_0}{q})^{\text{opt}}$  for various MCSs (numbers besides the markers denote the corresponding code rates; two receive antennas, DFD feedback length  $P = 1$ , ESTT EI, shadowing spread  $\sigma_s = 4.3\text{dB}$ , fast shadowing model, normalized Doppler frequency  $f_d T_s = 0.05$ )

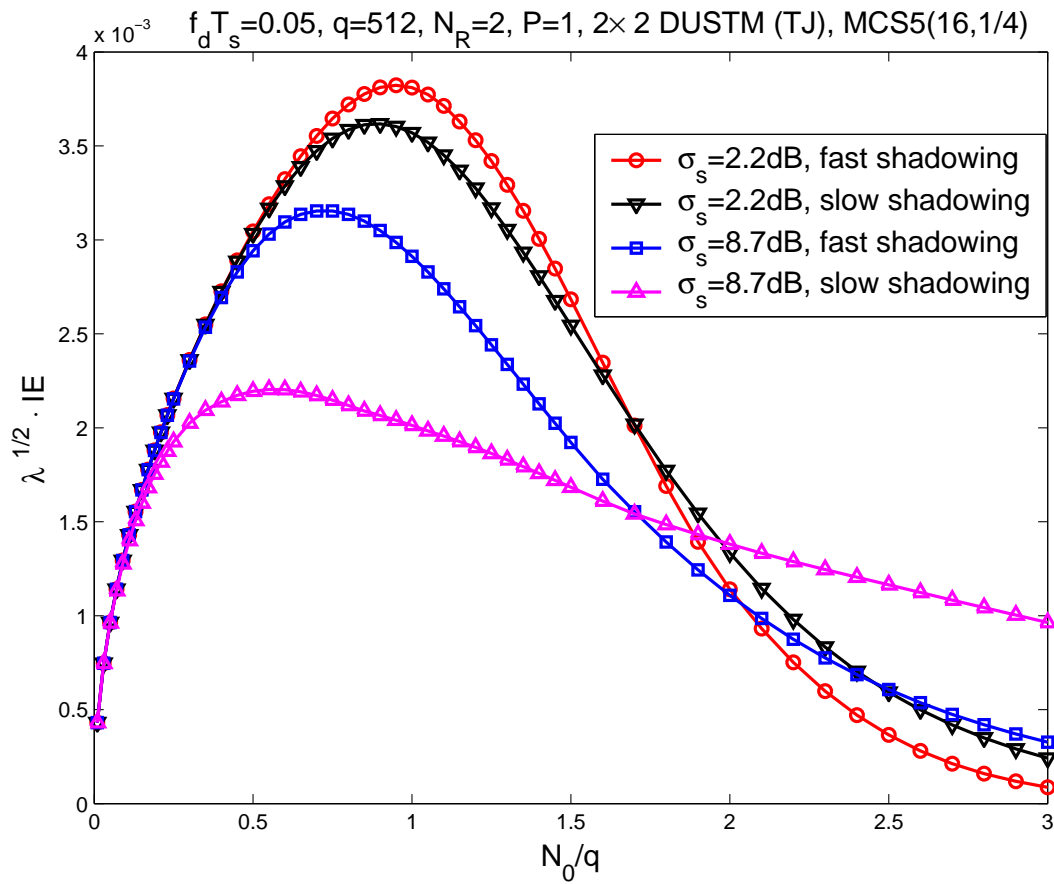


Fig. 6.  $\sqrt{\lambda IE}$  versus the expected number of in-range nodes per bandwidth  $\frac{N_0}{q}$  for different shadowing models (constellation size  $L = 16$ , rate- $\frac{1}{4}$  RS code, two receive antennas, DFD feedback length  $P = 1$ , ESTT EI, normalized Doppler frequency  $f_d T_s = 0.05$ )

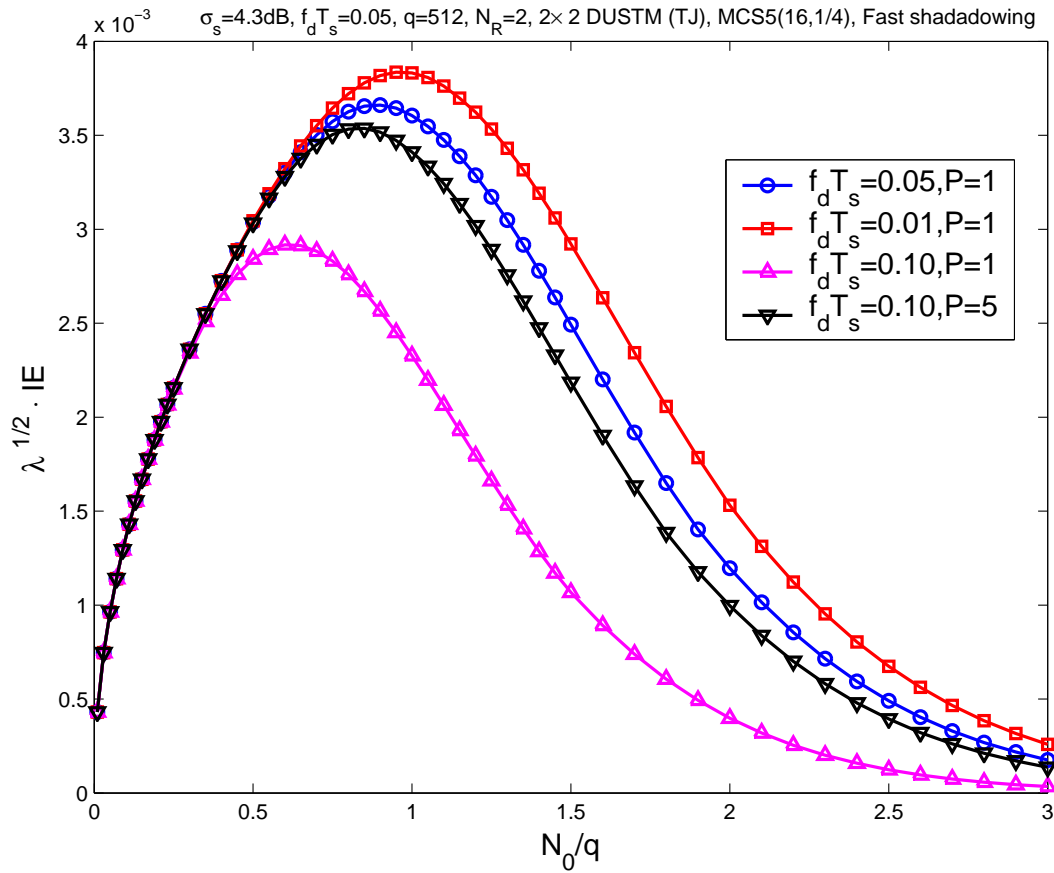


Fig. 7.  $\sqrt{\lambda}IE$  versus the expected number of in-range nodes per bandwidth  $\frac{N_0}{q}$  for different mobility ( $f_d T_s$ ) and DFD feedback length  $P$  (constellation size  $L = 16$ , rate- $\frac{1}{4}$  RS code, two receive antennas, ESTT EI, shadowing spread  $\sigma_s = 4.3\text{dB}$ , fast shadowing model)

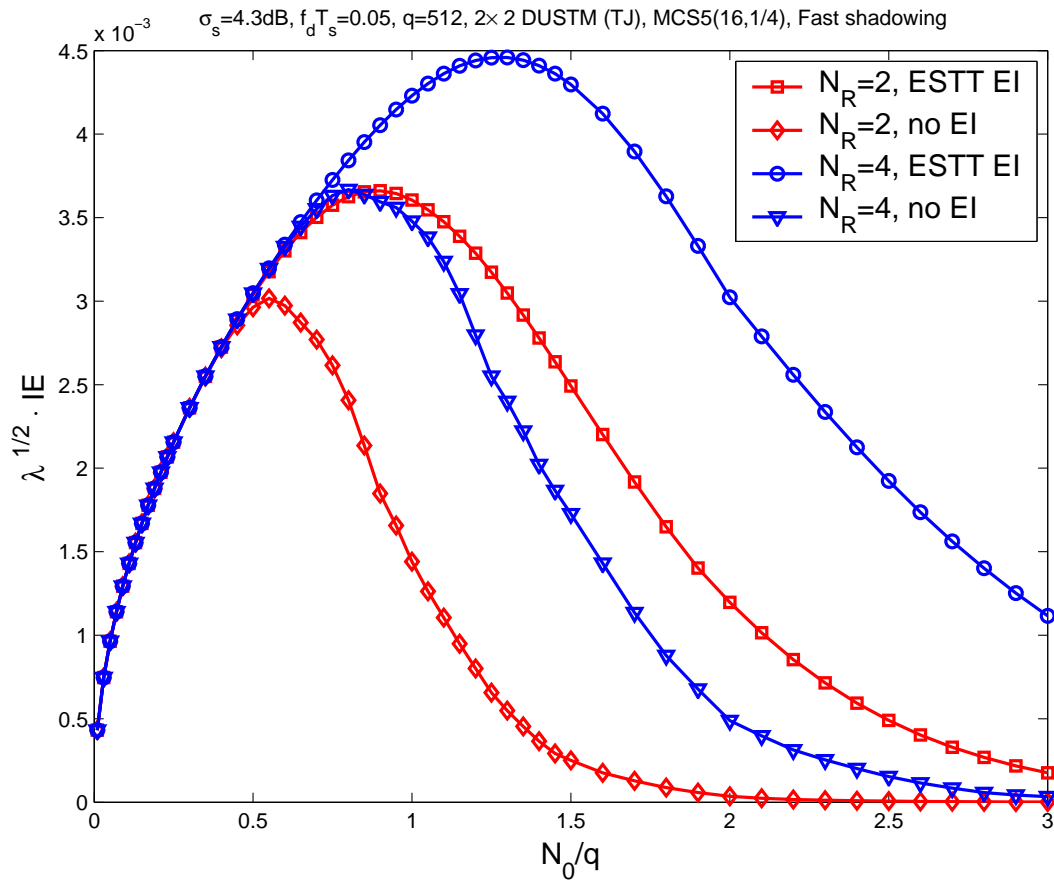


Fig. 8.  $\sqrt{\lambda IE}$  versus the expected number of in-range nodes per bandwidth  $\frac{N_0}{q}$  for different receive antenna numbers and with/without EI (constellation size  $L = 16$ , rate- $\frac{1}{4}$  RS code, shadowing spread  $\sigma_s = 4.3\text{dB}$ , fast shadowing model, normalized Doppler frequency  $f_d T_s = 0.05$ )